ORIGINAL ARTICLE

Analyzing three-dimensional wave propagation with the hybrid reproducing kernel particle method based on the dimension splitting method

Piaopiao Peng[1] · Yumin Cheng[1]

Abstract

By introducing the dimension splitting method into the reproducing kernel particle method (RKPM), a hybrid reproducing kernel particle method (HRKPM) for solving three-dimensional (3D) wave propagation problems is presented in this paper. Compared with the RKPM of 3D problems, the HRKPM needs only solving a set of two-dimensional (2D) problems in some subdomains, rather than solving a 3D problem in the 3D problem domain. The shape functions of 2D problems are much simpler than those of 3D problems, which results in that the HRKPM can save the CPU time greatly. Four numerical examples are selected to verify the validity and advantages of the proposed method. In addition, the error analysis and convergence of the proposed method are investigated. From the numerical results we can know that the HRKPM has higher computational efficiency than the RKPM and the element-free Galerkin method.

Keywords Meshless method · Dimension splitting method · Reproducing kernel particle method · Hybrid reproducing kernel particle method · Wave propagation

1 Introduction

Wave propagation exists in engineering fields, thus it is necessary to find efficient techniques for solving wave equations. Until now, the most commonly used approaches for these problems are the finite difference method [1–4] and the finite element method [5–7].

Meshless technique is a promising method, and its approximation function is based on a set of nodes [8–11]. Compared with the conventional numerical methods that need meshing the problem domain or boundary, the meshless methods do not require constant mesh reconstruction, so they will not cause the disadvantages of time consuming or sometimes difficult to use when dealing with some complicated problems [12–15]. Thus, the meshless methods are available to solve wave propagation problems. As one of the most widely used meshless methods, the element-free

✉ Yumin Cheng
  ymcheng@shu.edu.cn

1 Shanghai Key Laboratory of Mechanics in Energy
   Engineering, Shanghai Institute of Applied Mathematics
   and Mechanics, School of Mechanics and Engineering
   Science, Shanghai University, Shanghai 200072, China

Galerkin (EFG) method which based on the moving least-squares (MLS) approximation has been used to solve the hyperbolic equation [16–18]. By orthogonalizing the basis functions, Zhang et al. employed the improved element-free Galerkin (IEFG) method for the solution of 3D wave equations [19]. Shivanian presented the meshless local Petrov–Galerkin (MLPG) method for solving 3D nonlinear wave equations [20]. Shivanian and Shaban studied the pseudospectral meshless radial point interpolation (PSMRPI) method which combined meshless methods with spectral collocation techniques to solve 3D wave equations [21]. Liew and Cheng presented the mesh-free kp-Ritz method for solving 3D wave equations [22]. Dehghan and Salehi also studied some special cases of the wave equations using the meshless technique [23, 24].

The reproducing kernel particle method (RKPM) used in this paper is one of the most important meshless methods which was developed from the smoothed particle hydrodynamics (SPH) method [25]. Cheng et al. studied diverse heat conduction problems using the RKPM [26, 27]. Ma et al. introduced the Hermit-type radial basis function into the RKPM to solve wave equations [28]. Dehghan and Abbaszadeh have done much research on the RKPM and applied this method to solve many problems [29, 30]. Like the MLS approximation,

the RKPM is the approximation based on scalar functions [31, 32]. Then the shape functions must be computed at every point, which will lead to large computational cost. Therefore, Chen et al. presented the complex variable reproducing kernel particle method (CVRKPM) which is the approximation based on vector function and applied it to some problems [33–36]. Weng et al. also applied the CVRKPM for inverse heat conduction [37] and variable coefficient advection–diffusion problems [38]. However, the shape functions used in the RKPM and the CVRKPM are more complicated than the ones in finite element method, so they have lower computational efficiency, especially for 3D problems. Therefore, it is urgent to improve the computational efficiency of meshless methods to solve 3D problems.

By transforming the procedure of solving a 3D problem into solving a group of 2D problems, Li et al. presented the dimension splitting method (DSM) for many kinds of 3D problems [39–41]. Bragin and Rogov dealt with multidimensional scalar quasilinear hyperbolic conservation law using the DSM [42]. Recently, some meshless methods, such as the improved complex variable element-free Galerkin (ICVEFG) method [43–47], the IEFG method [48–50] and the RKPM [51], are combined with the DSM to form some approaches that can overcome the inefficiency of the meshless methods in solving 3D problems. And all these papers show a great improvement in computational efficiency.

By introducing the DSM into the RKPM, a hybrid reproducing kernel particle method (HRKPM) for solving 3D wave propagation problems is presented in this paper. Compared with the RKPM of 3D problems, the HRKPM needs only solving a set of 2D problems in some subdomains, rather than solving a 3D problem in the 3D problem domain. The shape functions of 2D problems are much simpler than those of 3D problems, which results in that the HRKPM can save the CPU time greatly. Four numerical examples are selected to verify the validity and advantages of the proposed method. In addition, the error analysis and convergence of the proposed method are investigated. From the numerical results we can know that the HRKPM has higher computational efficiency than the RKPM and the EFG method.

2 Basic equations in HRKPM scheme

In a 3D domain Ω with the boundary Γ, the hyperbolic equation governing the wave propagation u is

$$\frac{\partial^2 u}{\partial t^2} + r\frac{\partial u}{\partial t} + \bar{k}u - c^2\left(\frac{\partial^2 u}{\partial x_1^2} + \frac{\partial^2 u}{\partial x_2^2} + \frac{\partial^2 u}{\partial x_3^2}\right) - f(x_1, x_2, x_3, t) = 0,$$

$$((x_1, x_2, x_3) \in \Omega, \quad t \in [0, T]), \tag{1}$$

the boundary conditions are

$$u(x_1, x_2, x_3, t) = \bar{u}(x_1, x_2, x_3, t), \quad ((x_1, x_2, x_3) \in \Gamma_u), \tag{2}$$

$$q(x_1, x_2, x_3, t) = c^2\left(\frac{\partial u}{\partial x_1}n_1 + \frac{\partial u}{\partial x_2}n_2 + \frac{\partial u}{\partial x_3}n_3\right)$$
$$= \mathbf{n} \cdot c^2 \nabla u(x_1, x_2, x_3, t) = \bar{q}(x_1, x_2, x_3, t),$$
$$((x_1, x_2, x_3) \in \Gamma_q), \tag{3}$$

and the initial conditions are

$$u(x_1, x_2, x_3, 0) = \phi_1(x_1, x_2, x_3), \tag{4}$$

$$\frac{\partial u(x_1, x_2, x_3, 0)}{\partial t} = \phi_2(x_1, x_2, x_3), \tag{5}$$

where c^2 denotes wave speed, r represents resistance, $\bar{k}$ is the coefficient of source term; t is time, T is the total time; $\mathbf{n} = (n_1, n_2, n_3)$ is the outward unit normal vector on the boundary Γ, Γ_u and Γ_q are essential boundary and natural boundary, respectively, $\Gamma = \Gamma_u \cup \Gamma_q$; $f(x_1, x_2, x_3, t)$ represents external applied force; and $\phi_1(x_1, x_2, x_3)$ and $\phi_2(x_1, x_2, x_3)$ are given functions.

This problem is a kind of classical mathematical and physical equations, and the corresponding existence and uniqueness of the solutions were analyzed [52].

Without loss of generality, we choose x_3 as the splitting direction. By introducing the DSM, the problem domain Ω can be divided into $L + 1$ layers in this direction as shown in Fig. 1. Then, there are $L + 1$ subdomains $\Omega^{(k)}$, $k = 0, 1, \ldots, L$ existed at the layer $x_3 = x_3^{(k)}$,

$$a = x_3^{(0)} < x_3^{(1)} < \cdots < x_3^{(L-1)} < x_3^{(L)} = b, \tag{6}$$

in which $x_3^{(k)}$ is the value of x_3 at the layer $x_3 = x_3^{(k)}$, a and b represent the values of x_3 at the layer $x_3 = x_3^{(0)}$ and $x_3 = x_3^{(L)}$, respectively; L is the step number.

At each layer $x_3 = x_3^{(k)}$, the plane rectangular coordinate system can be expressed as $O^{(k)}x_1x_2$, and the origin is $O^{(k)}(0, 0, x_3^{(k)})$.

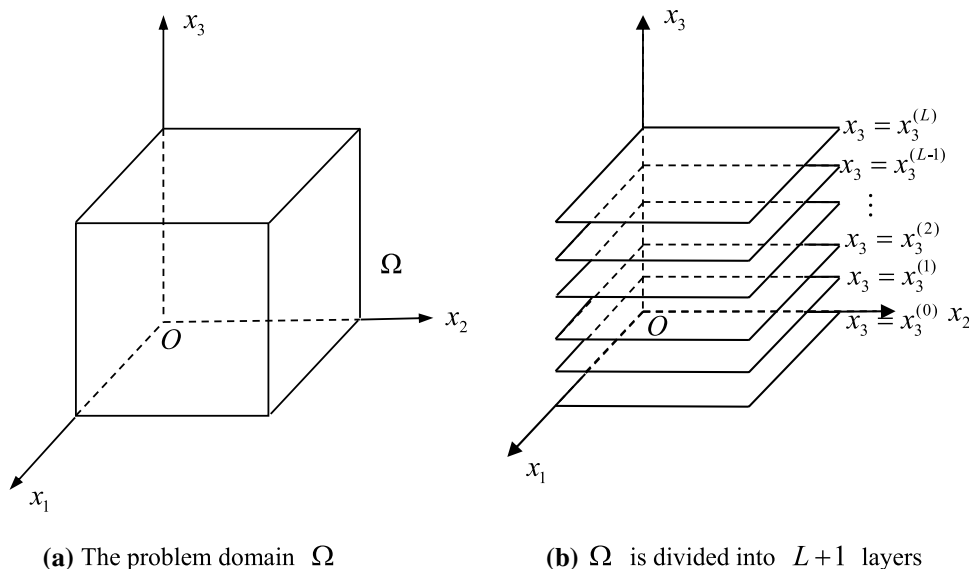The relationship between Ω and $\Omega^{(k)}$ can be expressed as

$$\Omega = \bigcup_{k=0}^{L-1}\left\{\Omega^{(k)} \times [x_3^{(k)}, x_3^{(k+1)})\right\} \cup \Omega^{(L)}, \tag{7}$$

where $[x_3^{(k)}, x_3^{(k+1)})$ $(k = 0, 1, \ldots, L-1)$ means the space between $\Omega^{(k)}$ and $\Omega^{(k+1)}$.

In the subdomain $\Omega^{(k)}$, the 2D wave propagation problem can be expressed as

$$\frac{\partial^2 u^{(k)}}{\partial t^2} + r\frac{\partial u^{(k)}}{\partial t} + \bar{k}u^{(k)} - c^2\left(\frac{\partial^2 u^{(k)}}{\partial x_1^2} + \frac{\partial^2 u^{(k)}}{\partial x_2^2}\right) = c^2\frac{\partial^2 u^{(k)}}{\partial x_3^2} + f^{(k)},$$

Fig. 1 The idea of dimension splitting method

(a) The problem domain Ω 　　　　　**(b)** Ω is divided into $L+1$ layers

$$((x_1, x_2) \in \Omega^{(k)}, \quad x_3 = x_3^{(k)}), \tag{8}$$

where

$$u^{(k)} = u(x_1, x_2, x_3^{(k)}, t), \tag{9}$$

$$f^{(k)} = f(x_1, x_2, x_3^{(k)}, t). \tag{10}$$

The corresponding boundary conditions are

$$u^{(k)}(x_1, x_2, t) = \overline{u}^{(k)}(x_1, x_2, t) = \overline{u}(x_1, x_2, x_3^{(k)}, t), \quad ((x_1, x_2) \in \Gamma_u^{(k)}), \tag{11}$$

$$q^{(k)}(x_1, x_2, t) = \overline{q}^{(k)}(x_1, x_2, t) = \overline{q}(x_1, x_2, x_3^{(k)}, t), \quad ((x_1, x_2) \in \Gamma_q^{(k)}), \tag{12}$$

and the initial conditions are

$$u(x_1, x_2, x_3^{(k)}, 0) = \phi_1(x_1, x_2, x_3^{(k)}), \tag{13}$$

$$\frac{\partial u(x_1, x_2, x_3^{(k)}, 0)}{\partial t} = \phi_2(x_1, x_2, x_3^{(k)}), \tag{14}$$

where $\Gamma^{(k)}$ is the boundary of subdomain $\Omega^{(k)}$, $\Gamma^{(k)} = \Gamma_u^{(k)} \cup \Gamma_q^{(k)}$.

Then, the foregoing 2D wave propagation problem can be solved by the RKPM of 2D problems.

The equivalent functional of Eqs. (8)–(14) can be written as

$$\Pi = \int_{\Omega^{(k)}} u^{(k)} \left[\frac{\partial^2 u^{(k)}}{\partial t^2} + r\frac{\partial u^{(k)}}{\partial t} + \frac{1}{2}\overline{k}u^{(k)} - c^2\frac{\partial^2 u^{(k)}}{\partial x_3^2} - f^{(k)} \right] d\Omega^{(k)}$$
$$+ \frac{1}{2}\int_{\Omega^{(k)}} \left[c^2\left(\frac{\partial u^{(k)}}{\partial x_1}\right)^2 + c^2\left(\frac{\partial u^{(k)}}{\partial x_2}\right)^2 \right] d\Omega^{(k)} - \int_{\Gamma_q^{(k)}} u^{(k)} \cdot \overline{q}^{(k)} d\Gamma^{(k)}. \tag{15}$$

Imposing essential boundary conditions by penalty function method

$$\Pi^* = \Pi + \frac{\alpha}{2}\int_{\Gamma_u^{(k)}} (u^{(k)} - \overline{u}^{(k)})(u^{(k)} - \overline{u}^{(k)})d\Gamma^{(k)}, \tag{16}$$

where α is the penalty factors.

The modified equivalent integral weak form is

$$\Pi^* = \int_{\Omega^{(k)}} u^{(k)} \left[\frac{\partial^2 u^{(k)}}{\partial t^2} + r\frac{\partial u^{(k)}}{\partial t} + \frac{1}{2}\overline{k} \cdot u^{(k)} - c^2\frac{\partial^2 u^{(k)}}{\partial x_3^2} - f^{(k)} \right] d\Omega^{(k)}$$
$$+ c^2\int_{\Omega^{(k)}} (\mathbf{L}u^{(k)})^{\mathrm{T}} \cdot (\mathbf{L}u^{(k)}) d\Omega^{(k)} - \int_{\Gamma_q^{(k)}} u^{(k)} \cdot \overline{q}^{(k)} d\Gamma^{(k)}$$
$$+ \int_{\Gamma_u^{(k)}} u^{(k)} \cdot \alpha(u^{(k)} - \overline{u}^{(k)}) d\Gamma^{(k)}, \tag{17}$$

where

$$\mathbf{L}(\,\cdot\,) = \begin{bmatrix} \frac{\partial}{\partial x_1} \\ \frac{\partial}{\partial x_2} \end{bmatrix}(\cdot). \tag{18}$$

3 The HRKPM for 3D wave propagation

3.1 The approximation function of the RKPM

Using the RKPM [26, 30], the approximation function of $u^{(k)}$ at any points $\mathbf{x} = (x_1, x_2) \in \Omega^{(k)}$ can be expressed as

$$u^h(\mathbf{x}, x_3^{(k)}, t) = \int_{\Omega^{(k)}} u(\mathbf{x}')\overline{w}(\mathbf{x} - \mathbf{x}')d\mathbf{x}', \tag{19}$$

where $\overline{w}(\mathbf{x} - \mathbf{x}')$ is the correction kernel function,

$$\overline{w}(\mathbf{x} - \mathbf{x}') = C(\mathbf{x};\mathbf{x} - \mathbf{x}')w(\mathbf{x} - \mathbf{x}'), \tag{20}$$

in which $w(\mathbf{x} - \mathbf{x}')$ is weight function which has a compact support domain, and $C(\mathbf{x}; \mathbf{x} - \mathbf{x}')$ is the correction function,

$$C(\mathbf{x};\mathbf{x} - \mathbf{x}') = \sum_{i=1}^{m} p_i(\mathbf{x} - \mathbf{x}')b_i(\mathbf{x}) = \mathbf{p}^{\mathrm{T}}(\mathbf{x} - \mathbf{x}')\mathbf{b}(\mathbf{x}), \quad (\mathbf{x} \in \Omega^{(k)}), \tag{21}$$

where m is the number of basis functions, $\mathbf{p}(\mathbf{x} - \mathbf{x}')$ is the vector of the basis functions $p_i(\mathbf{x} - \mathbf{x}')$, $(i = 1, 2, \ldots, m)$; and $b_i(\mathbf{x})$ are the coefficients of basis functions, $\mathbf{b}(\mathbf{x})$ is the vector of the coefficients,

$$\mathbf{b}(\mathbf{x}) = (b_1(\mathbf{x}), b_2(\mathbf{x}), \ldots, b_m(\mathbf{x}))^{\mathrm{T}}. \tag{22}$$

In general, the basis function can be chosen as linear basis,

$$\mathbf{p}^{\mathrm{T}} = (1, x_1 - x_1', x_2 - x_2'), \tag{23}$$

or quadratic basis,

$$\mathbf{p}^{\mathrm{T}} = (1, x_1 - x_1', x_2 - x_2', (x_1 - x_1')^2, (x_1 - x_1')(x_2 - x_2'), (x_2 - x_2')^2). \tag{24}$$

The trapezoidal integral method is used to obtain the discretization approximation, and then Eq. (19) can be written as

$$u^h(\mathbf{x}, x_3^{(k)}, t) = \sum_{I=1}^{n} C(\mathbf{x};\mathbf{x} - \mathbf{x}_I)w(\mathbf{x} - \mathbf{x}_I)u_I^{(k)}\Delta V_I, \tag{25}$$

where $\mathbf{x}_I$ $(I = 1, 2, \ldots, n)$ are nodes in the neighborhood of the point $\mathbf{x}$, $u_I^{(k)}$ is the value of $u^{(k)}$ at the node $\mathbf{x}_I$,

$$u_I^{(k)} = u(\mathbf{x}_I, x_3^{(k)}, t), \quad I = 1, 2, \ldots, n; \tag{26}$$

and ΔV is a regional measure related to $\mathbf{x}_I$,

$$\sum_{I=1}^{n} \Delta V_I = \mathbf{V}. \tag{27}$$

The matrix form of Eq. (25) can be expressed as

$$u^h(\mathbf{x}, x_3^{(k)}, t) = \mathbf{C}(\mathbf{x})\mathbf{W}(\mathbf{x})\mathbf{V}\mathbf{u}, \tag{28}$$

where $\mathbf{u}$ is the vector of the variable at the nodes,

$$\mathbf{u} = (u_1^{(k)}, u_2^{(k)}, \ldots, u_n^{(k)})^{\mathrm{T}}, \tag{29}$$

$\mathbf{W}(\mathbf{x})$ is the matrix of weight functions,

$$\mathbf{W}(\mathbf{x}) = \begin{bmatrix} w(\mathbf{x} - \mathbf{x}_1) & 0 & \cdots & 0 \\ 0 & w(\mathbf{x} - \mathbf{x}_2) & \cdots & 0 \\ \vdots & \vdots & \ddots & \vdots \\ 0 & 0 & \cdots & w(\mathbf{x} - \mathbf{x}_n) \end{bmatrix}, \tag{30}$$

$\mathbf{V}$ is the matrix of regional measures related to $\mathbf{x}_I$,

$$\mathbf{V} = \begin{bmatrix} \Delta V_1 & 0 & \cdots & 0 \\ 0 & \Delta V_2 & \cdots & 0 \\ \vdots & \vdots & \ddots & \vdots \\ 0 & 0 & \cdots & \Delta V_n \end{bmatrix}, \tag{31}$$

$\mathbf{C}(\mathbf{x})$ is the vector of correction functions,

$$\mathbf{C}(\mathbf{x}) = (C_1(\mathbf{x}), C_2(\mathbf{x}), \ldots, C_n(\mathbf{x})) = \mathbf{b}^{\mathrm{T}}(\mathbf{x})\mathbf{P}, \tag{32}$$

$$C_I(\mathbf{x}) = C(\mathbf{x};\mathbf{x} - \mathbf{x}_I), \tag{33}$$

and $\mathbf{P}$ is the matrix of basis functions,

$$\mathbf{P} = \begin{bmatrix} p_1(\mathbf{x} - \mathbf{x}_1) & p_1(\mathbf{x} - \mathbf{x}_2) & \cdots & p_1(\mathbf{x} - \mathbf{x}_n) \\ p_2(\mathbf{x} - \mathbf{x}_1) & p_2(\mathbf{x} - \mathbf{x}_2) & \cdots & p_2(\mathbf{x} - \mathbf{x}_n) \\ \vdots & \vdots & \ddots & \vdots \\ p_m(\mathbf{x} - \mathbf{x}_1) & p_m(\mathbf{x} - \mathbf{x}_2) & \cdots & p_m(\mathbf{x} - \mathbf{x}_n) \end{bmatrix}. \tag{34}$$

The coefficients $b_i(\mathbf{x})$ are determined by the reproducing conditions of the approximation function. Let

$$\overline{\mathbf{M}}(\mathbf{x}) = \mathbf{M}(\mathbf{x})\mathbf{b}(\mathbf{x}) = \mathbf{H}, \tag{35}$$

where

$$\mathbf{M}(\mathbf{x}) = \sum_{I=1}^{n} \mathbf{p}(\mathbf{x} - \mathbf{x}_I)\mathbf{p}^{\mathrm{T}}(\mathbf{x} - \mathbf{x}_I)w(\mathbf{x} - \mathbf{x}_I)\Delta V_I, \tag{36}$$

$$\mathbf{H} = (1, 0, \ldots, 0)^{\mathrm{T}}, \tag{37}$$

then we have

$$\mathbf{b}(\mathbf{x}) = \mathbf{M}^{-1}(\mathbf{x})\mathbf{H}. \tag{38}$$

Finally, the approximation function $u^h(\mathbf{x}, x_3^{(k)}, t)$ is obtained as

$$u^h(\mathbf{x}, x_3^{(k)}, t) = \sum_{I=1}^{n} \Phi_I^{(k)}(\mathbf{x})u_I^{(k)} = \mathbf{\Phi}(\mathbf{x})\mathbf{u}, \quad k = 0, 1, \ldots, L, \tag{39}$$

where $\mathbf{\Phi}(\mathbf{x})$ is the shape function,

$$\mathbf{\Phi}(\mathbf{x}) = (\Phi_1^{(k)}(\mathbf{x}), \Phi_2^{(k)}(\mathbf{x}), \ldots, \Phi_n^{(k)}(\mathbf{x})) = \mathbf{C}(\mathbf{x})\mathbf{W}(\mathbf{x})\mathbf{V}. \tag{40}$$

3.2 The discretized equation of the HRKPM for 3D wave propagation

According to Eq. (39), we can obtain the following approximations related to $u^{(k)}$,

$$\frac{\partial^2 u^{(k)}}{\partial x_3^2} = \frac{\partial}{\partial x_3^2} \sum_{I=1}^{n} \Phi_I^{(k)}(\mathbf{x}) \cdot u_I^{(k)} = \sum_{I=1}^{n} \Phi_I^{(k)}(\mathbf{x}) \frac{\partial^2 u_I^{(k)}}{\partial x_3^2} = \mathbf{\Phi}(\mathbf{x}) D_{x_3 x_3} \mathbf{u}, \tag{41}$$

$$\frac{\partial u^{(k)}}{\partial t} = \frac{\partial}{\partial t} \sum_{I=1}^{n} \Phi_I^{(k)}(\mathbf{x}) \cdot u_I^{(k)} = \sum_{I=1}^{n} \Phi_I^{(k)}(\mathbf{x}) \frac{\partial u_I^{(k)}}{\partial t} = \mathbf{\Phi}(\mathbf{x}) \dot{\mathbf{u}}, \tag{42}$$

$$\frac{\partial^2 u^{(k)}}{\partial t^2} = \frac{\partial^2}{\partial t^2} \sum_{I=1}^{n} \Phi_I^{(k)}(\mathbf{x}) \cdot u_I^{(k)} = \sum_{I=1}^{n} \Phi_I^{(k)}(\mathbf{x}) \frac{\partial^2 u_I^{(k)}}{\partial t^2} = \mathbf{\Phi}(\mathbf{x}) \ddot{\mathbf{u}}, \tag{43}$$

$$\mathbf{L} u^{(k)} = \sum_{I=1}^{n} \begin{bmatrix} \frac{\partial}{\partial x_1} \\ \frac{\partial}{\partial x_2} \end{bmatrix} \Phi_I^{(k)}(\mathbf{x}) \cdot u_I^{(k)} = \sum_{I=1}^{n} \mathbf{B}_I^{(k)}(\mathbf{x}) u_I^{(k)} = \mathbf{B}(\mathbf{x}) \mathbf{u}, \tag{44}$$

where

$$D_{x_3 x_3} \mathbf{u} = \left(\frac{\partial^2 u_1^{(k)}}{\partial x_3^2}, \frac{\partial^2 u_2^{(k)}}{\partial x_3^2}, \ldots, \frac{\partial^2 u_n^{(k)}}{\partial x_3^2} \right)^{\mathrm{T}}, \tag{45}$$

$$\dot{\mathbf{u}} = \left(\frac{\partial u_1^{(k)}}{\partial t}, \frac{\partial u_2^{(k)}}{\partial t}, \ldots, \frac{\partial u_n^{(k)}}{\partial t} \right)^{\mathrm{T}}, \tag{46}$$

$$\ddot{\mathbf{u}} = \left(\frac{\partial^2 u_1^{(k)}}{\partial t^2}, \frac{\partial^2 u_2^{(k)}}{\partial t^2}, \ldots, \frac{\partial^2 u_n^{(k)}}{\partial t^2} \right)^{\mathrm{T}}, \tag{47}$$

$$\mathbf{B}(\mathbf{x}) = (\mathbf{B}_1^{(k)}(\mathbf{x}), \mathbf{B}_2^{(k)}(\mathbf{x}), \ldots, \mathbf{B}_n^{(k)}(\mathbf{x})), \tag{48}$$

$$\mathbf{B}_I^{(k)}(\mathbf{x}) = \begin{bmatrix} \Phi_{I,1}^{(k)}(\mathbf{x}) \\ \Phi_{I,2}^{(k)}(\mathbf{x}) \end{bmatrix}. \tag{49}$$

Substitute Eqs. (41)–(44) into Eq. (17) yields

$$\Pi^* = \int_{\Omega^{(k)}} [\mathbf{B}(\mathbf{x})\mathbf{u}]^{\mathrm{T}} \cdot c^2 \cdot [\mathbf{B}(\mathbf{x})\mathbf{u}] d\Omega^{(k)} + \int_{\Omega^{(k)}} \mathbf{\Phi}(\mathbf{x})\mathbf{u} \cdot \mathbf{\Phi}(\mathbf{x})\ddot{\mathbf{u}} d\Omega^{(k)}$$
$$+ \int_{\Omega^{(k)}} \mathbf{\Phi}(\mathbf{x})\mathbf{u} \cdot r \cdot \mathbf{\Phi}(\mathbf{x})\dot{\mathbf{u}} d\Omega^{(k)} + \frac{1}{2} \int_{\Omega^{(k)}} \mathbf{\Phi}(\mathbf{x})\mathbf{u} \cdot \bar{k} \cdot \mathbf{\Phi}(\mathbf{x})\mathbf{u} d\Omega^{(k)}$$
$$- \int_{\Omega^{(k)}} \mathbf{\Phi}(\mathbf{x})\mathbf{u} \cdot c^2 \cdot \mathbf{\Phi}(\mathbf{x}) D_{x_3 x_3} \mathbf{u} d\Omega^{(k)} - \int_{\Omega^{(k)}} \mathbf{\Phi}(\mathbf{x})\mathbf{u} \cdot f^{(k)} d\Omega^{(k)}$$
$$- \int_{\Gamma_q^{(k)}} \mathbf{\Phi}(\mathbf{x})\mathbf{u} \cdot \bar{q}^{(k)} d\Gamma^{(k)} + \int_{\Gamma_u^{(k)}} \mathbf{\Phi}(\mathbf{x})\mathbf{u} \cdot \alpha \cdot \mathbf{\Phi}(\mathbf{x})\mathbf{u} d\Gamma^{(k)}$$
$$- \int_{\Gamma_u^{(k)}} \mathbf{\Phi}(\mathbf{x})\mathbf{u} \cdot \alpha \cdot \bar{u}^{(k)} d\Gamma^{(k)}. \tag{50}$$

The variation formulation of Eq. (50) is

$$\delta\Pi^* = \int_{\Omega^{(k)}} \delta\mathbf{u}^{\mathrm{T}} \left[\mathbf{B}^{\mathrm{T}}(\mathbf{x}) \cdot c^2 \cdot \mathbf{B}(\mathbf{x}) \right] \mathbf{u} d\Omega^{(k)} + \int_{\Omega^{(k)}} \delta\mathbf{u}^{\mathrm{T}} \left[\mathbf{\Phi}^{\mathrm{T}}(\mathbf{x}) \cdot \mathbf{\Phi}(\mathbf{x}) \right] \ddot{\mathbf{u}} d\Omega^{(k)}$$
$$+ \int_{\Omega^{(k)}} \delta\mathbf{u}^{\mathrm{T}} \left[\mathbf{\Phi}^{\mathrm{T}}(\mathbf{x}) \cdot r \cdot \mathbf{\Phi}(\mathbf{x}) \right] \dot{\mathbf{u}} d\Omega^{(k)} + \bar{k} \int_{\Omega^{(k)}} \delta\mathbf{u}^{\mathrm{T}} \left[\mathbf{\Phi}^{\mathrm{T}}(\mathbf{x}) \cdot \mathbf{\Phi}(\mathbf{x}) \right] \mathbf{u} d\Omega^{(k)}$$
$$- \int_{\Omega^{(k)}} \delta\mathbf{u}^{\mathrm{T}} \left[\mathbf{\Phi}^{\mathrm{T}}(\mathbf{x}) \cdot c^2 \cdot \mathbf{\Phi}(\mathbf{x}) \right] D_{x_3 x_3} \mathbf{u} d\Omega^{(k)} - \int_{\Omega^{(k)}} \delta\mathbf{u}^{\mathrm{T}} \left[\mathbf{\Phi}^{\mathrm{T}}(\mathbf{x}) \cdot f^{(k)} \right] d\Omega^{(k)}$$
$$- \int_{\Gamma_q^{(k)}} \delta\mathbf{u}^{\mathrm{T}} \left[\mathbf{\Phi}^{\mathrm{T}}(\mathbf{x}) \cdot \bar{q}^{(k)} \right] d\Gamma^{(k)} + \int_{\Gamma_u^{(k)}} \delta\mathbf{u}^{\mathrm{T}} \left[\mathbf{\Phi}^{\mathrm{T}}(\mathbf{x}) \cdot \alpha \cdot \mathbf{\Phi}(\mathbf{x}) \right] \mathbf{u} d\Gamma^{(k)}$$
$$- \int_{\Gamma_u^{(k)}} \delta\mathbf{u}^{\mathrm{T}} \left[\mathbf{\Phi}^{\mathrm{T}}(\mathbf{x}) \cdot \alpha \cdot \bar{u}^{(k)} \right] d\Gamma^{(k)}. \tag{51}$$

Since $\delta\mathbf{u}$ is arbitrary, from $\delta\Pi^* = 0$, the discrete system equation can be obtained as

$$\mathbf{C}\ddot{\mathbf{u}} + r\mathbf{C}\dot{\mathbf{u}} - c^2 \mathbf{C} D_{x_3 x_3} \mathbf{u} + \hat{\mathbf{K}}\mathbf{u} = \hat{\mathbf{F}}, \tag{52}$$

where

$$\hat{\mathbf{K}} = \mathbf{K} + \bar{k}\mathbf{C} + \mathbf{K}^\alpha, \tag{53}$$

$$\hat{\mathbf{F}} = \mathbf{F}^{(1)} + \mathbf{F}^{(2)} + \mathbf{F}^\alpha, \tag{54}$$

$$\mathbf{C} = \int_{\Omega^{(k)}} \mathbf{\Phi}^{\mathrm{T}}(\mathbf{x}) \mathbf{\Phi}(\mathbf{x}) d\Omega^{(k)}, \tag{55}$$

$$\mathbf{K} = c^2 \int_{\Omega^{(k)}} \mathbf{B}^{\mathrm{T}}(\mathbf{x}) \mathbf{B}(\mathbf{x}) d\Omega^{(k)}, \tag{56}$$

$$\mathbf{K}^\alpha = \alpha \int_{\Gamma_u^{(k)}} \mathbf{\Phi}^{\mathrm{T}}(\mathbf{x}) \mathbf{\Phi}(\mathbf{x}) d\Gamma^{(k)}, \tag{57}$$

$$\mathbf{F}^{(1)} = \int_{\Omega^{(k)}} \mathbf{\Phi}^{\mathrm{T}}(\mathbf{x}) f^{(k)} \mathrm{d}\Omega^{(k)}, \tag{58}$$

$$\mathbf{F}^{(2)} = \int_{\Gamma_q^{(k)}} \mathbf{\Phi}^{\mathrm{T}}(\mathbf{x}) \overline{q}^{(k)} \mathrm{d}\Gamma^{(k)}, \tag{59}$$

$$\mathbf{F}^{\alpha} = \alpha \int_{\Gamma_u^{(k)}} \mathbf{\Phi}^{\mathrm{T}}(\mathbf{x}) \overline{u}^{(k)} \mathrm{d}\Gamma^{(k)}. \tag{60}$$

According to finite difference method, we have

$$D_{x_3 x_3} \mathbf{u} \approx \frac{\mathbf{u}^{(k-1)} - 2\mathbf{u}^{(k)} + \mathbf{u}^{(k+1)}}{(\Delta x_3)^2}, \quad k = 1, 2, \ldots, L-1. \tag{61}$$

Then Eq. (52) can be written as

$$\mathbf{C}\ddot{\mathbf{u}}^{(k)} + r\mathbf{C}\dot{\mathbf{u}}^{(k)} - c^2\mathbf{C}\frac{\mathbf{u}^{(k-1)} - 2\mathbf{u}^{(k)} + \mathbf{u}^{(k+1)}}{(\Delta x_3)^2} + \hat{\mathbf{K}}\mathbf{u}^{(k)} = \hat{\mathbf{F}}. \tag{62}$$

And the discrete system formulas in each subdomain can be expressed as

$$\mathbf{C}\ddot{\mathbf{u}}^{(1)} + r\mathbf{C}\dot{\mathbf{u}}^{(1)} - c^2\mathbf{C}\frac{\mathbf{u}^{(0)} - 2\mathbf{u}^{(1)} + \mathbf{u}^{(2)}}{(\Delta x_3)^2} + \hat{\mathbf{K}}\mathbf{u}^{(1)} = \hat{\mathbf{F}}^{(1)}, \tag{63}$$

$$\mathbf{C}\ddot{\mathbf{u}}^{(2)} + r\mathbf{C}\dot{\mathbf{u}}^{(2)} - c^2\mathbf{C}\frac{\mathbf{u}^{(1)} - 2\mathbf{u}^{(2)} + \mathbf{u}^{(3)}}{(\Delta x_3)^2} + \hat{\mathbf{K}}\mathbf{u}^{(2)} = \hat{\mathbf{F}}^{(2)}, \tag{64}$$

$$\mathbf{C}\ddot{\mathbf{u}}^{(3)} + r\mathbf{C}\dot{\mathbf{u}}^{(3)} - c^2\mathbf{C}\frac{\mathbf{u}^{(2)} - 2\mathbf{u}^{(3)} + \mathbf{u}^{(4)}}{(\Delta x_3)^2} + \hat{\mathbf{K}}\mathbf{u}^{(3)} = \hat{\mathbf{F}}^{(3)}, \tag{65}$$

$$\vdots$$

$$\mathbf{C}\ddot{\mathbf{u}}^{(L-2)} + r\mathbf{C}\dot{\mathbf{u}}^{(L-2)} - c^2\mathbf{C}\frac{\mathbf{u}^{(L-3)} - 2\mathbf{u}^{(L-2)} + \mathbf{u}^{(L-1)}}{(\Delta x_3)^2} + \hat{\mathbf{K}}\mathbf{u}^{(L-2)} = \hat{\mathbf{F}}^{(L-2)}, \tag{66}$$

$$\mathbf{C}\ddot{\mathbf{u}}^{(L-1)} + r\mathbf{C}\dot{\mathbf{u}}^{(L-1)} - c^2\mathbf{C}\frac{\mathbf{u}^{(L-2)} - 2\mathbf{u}^{(L-1)} + \mathbf{u}^{(L)}}{(\Delta x_3)^2} + \hat{\mathbf{K}}\mathbf{u}^{(L-1)} = \hat{\mathbf{F}}^{(L-1)}, \tag{67}$$

where

$$\mathbf{u}^{(k)} = \mathbf{u}(\mathbf{x}, x_3^{(k)}, t), \tag{68}$$

$$\mathbf{u}^{(0)} = \mathbf{u}(\mathbf{x}, a, t), \tag{69}$$

$$\mathbf{u}^{(L)} = \mathbf{u}(\mathbf{x}, b, t), \tag{70}$$

$$\Delta x_3 = x_3^{(k)} - x_3^{(k-1)} = (b-a)/L. \tag{71}$$

The matrix form of Eqs. (63)-(67) is

$$\mathbf{R}\begin{bmatrix} \ddot{\mathbf{u}}^{(1)} \\ \ddot{\mathbf{u}}^{(2)} \\ \ddot{\mathbf{u}}^{(3)} \\ \vdots \\ \ddot{\mathbf{u}}^{(L-2)} \\ \ddot{\mathbf{u}}^{(L-1)} \end{bmatrix} + r\mathbf{R}\begin{bmatrix} \dot{\mathbf{u}}^{(1)} \\ \dot{\mathbf{u}}^{(2)} \\ \dot{\mathbf{u}}^{(3)} \\ \vdots \\ \dot{\mathbf{u}}^{(L-2)} \\ \dot{\mathbf{u}}^{(L-1)} \end{bmatrix} - \tilde{k}\begin{bmatrix} \mathbf{H} & \mathbf{C} & & & & \\ \mathbf{C} & \mathbf{H} & \mathbf{C} & & & \\ & \mathbf{C} & \mathbf{H} & \mathbf{C} & & \\ & & \ddots & \ddots & \ddots & \\ & & & \mathbf{C} & \mathbf{H} & \mathbf{C} \\ & & & & \mathbf{C} & \mathbf{H} \end{bmatrix}\begin{bmatrix} \mathbf{u}^{(1)} \\ \mathbf{u}^{(2)} \\ \mathbf{u}^{(3)} \\ \vdots \\ \mathbf{u}^{(L-2)} \\ \mathbf{u}^{(L-1)} \end{bmatrix} = \begin{bmatrix} \hat{\mathbf{F}}^{(1)} + \mathbf{M} \\ \hat{\mathbf{F}}^{(2)} \\ \hat{\mathbf{F}}^{(3)} \\ \vdots \\ \hat{\mathbf{F}}^{(L-2)} \\ \hat{\mathbf{F}}^{(L-1)} + \mathbf{W} \end{bmatrix}, \tag{72}$$

where

$$\tilde{k} = \frac{c^2}{(\Delta x_3)^2}, \tag{73}$$

$$\mathbf{M} = \frac{c^2 \mathbf{C} \mathbf{u}^{(0)}}{(\Delta x_3)^2}, \tag{74}$$

$$\mathbf{W} = \frac{c^2 \mathbf{C} \mathbf{u}^{(L)}}{(\Delta x_3)^2}, \tag{75}$$

$$\mathbf{R} = \begin{bmatrix} \mathbf{C} & & & & & \\ & \mathbf{C} & & & & \\ & & \mathbf{C} & & & \\ & & & \ddots & & \\ & & & & \mathbf{C} & \\ & & & & & \mathbf{C} \end{bmatrix}, \tag{76}$$

$$\mathbf{H} = -2\mathbf{C} - \frac{(\Delta x_3)^2}{c^2}\hat{\mathbf{K}}. \tag{77}$$

Let

$$\tilde{\mathbf{u}} = \left(\mathbf{u}^{(1)^{\mathrm{T}}}, \mathbf{u}^{(2)^{\mathrm{T}}}, \mathbf{u}^{(3)^{\mathrm{T}}}, \ldots, \mathbf{u}^{(L-2)^{\mathrm{T}}}, \mathbf{u}^{(L-1)^{\mathrm{T}}} \right)^{\mathrm{T}}, \tag{78}$$

$$\ddot{\tilde{\mathbf{u}}} = \left(\ddot{\mathbf{u}}^{(1)^{\mathrm{T}}}, \ddot{\mathbf{u}}^{(2)^{\mathrm{T}}}, \ddot{\mathbf{u}}^{(3)^{\mathrm{T}}}, \ldots, \ddot{\mathbf{u}}^{(L-2)^{\mathrm{T}}}, \ddot{\mathbf{u}}^{(L-1)^{\mathrm{T}}} \right)^{\mathrm{T}}, \tag{79}$$

$$\dot{\tilde{\mathbf{u}}} = \left(\dot{\mathbf{u}}^{(1)^{\mathrm{T}}}, \dot{\mathbf{u}}^{(2)^{\mathrm{T}}}, \dot{\mathbf{u}}^{(3)^{\mathrm{T}}}, \ldots, \dot{\mathbf{u}}^{(L-2)^{\mathrm{T}}}, \dot{\mathbf{u}}^{(L-1)^{\mathrm{T}}} \right)^{\mathrm{T}}, \tag{80}$$

$$\mathbf{E} = \tilde{k}\begin{bmatrix} \mathbf{H} & \mathbf{C} & & & & \\ \mathbf{C} & \mathbf{H} & \mathbf{C} & & & \\ & \mathbf{C} & \mathbf{H} & \mathbf{C} & & \\ & & \ddots & \ddots & \ddots & \\ & & & \mathbf{C} & \mathbf{H} & \mathbf{C} \\ & & & & \mathbf{C} & \mathbf{H} \end{bmatrix}, \tag{81}$$

$$\mathbf{G} = ((\hat{\mathbf{F}}^{(1)} + \mathbf{M})^{\mathrm{T}}, \hat{\mathbf{F}}^{(2)^{\mathrm{T}}}, \hat{\mathbf{F}}^{(3)^{\mathrm{T}}}, \ldots, \hat{\mathbf{F}}^{(L-2)^{\mathrm{T}}}, (\hat{\mathbf{F}}^{(L-1)} + \mathbf{W})^{\mathrm{T}})^{\mathrm{T}}. \tag{82}$$

Equation (72) can be derived as following equation

$$\mathbf{R}\ddot{\tilde{\mathbf{u}}} + r\mathbf{R}\dot{\tilde{\mathbf{u}}} - \mathbf{E}\tilde{\mathbf{u}} = \mathbf{G}. \tag{83}$$

We obtain the time discretization of Eq. (83) by the center difference method

$$\mathbf{R}\frac{\tilde{\mathbf{u}}^{(i+2)} - 2\tilde{\mathbf{u}}^{(i+1)} + \tilde{\mathbf{u}}^{(i)}}{(\Delta t)^2} + r\mathbf{R}\frac{\tilde{\mathbf{u}}^{(i+1)} - \tilde{\mathbf{u}}^{(i)}}{\Delta t} - \mathbf{E}\frac{\tilde{\mathbf{u}}^{(i+1)} + \tilde{\mathbf{u}}^{(i)}}{2} = \mathbf{G}, \tag{84}$$

that is

$$2\mathbf{R}\tilde{\mathbf{u}}^{(i+2)} = (4\mathbf{R} - 2r\Delta t\mathbf{R} + (\Delta t)^2\mathbf{E})\tilde{\mathbf{u}}^{(i+1)}$$
$$+ (2r\Delta t\mathbf{R} + (\Delta t)^2\mathbf{E} - 2\mathbf{R})\tilde{\mathbf{u}}^{(i)} + 2(\Delta t)^2\mathbf{G}, \tag{85}$$

where Δt represents time step length.

4 Numerical examples

To test whether the proposed method can improve the computational efficiency, the numerical results of the following examples obtained by the HRKPM are compared with analytical ones and the ones of the RKPM and the EFG method.

4.1 Wave propagation problem with Dirichlet boundary conditions

In the 3D domain $\Omega = [0, \pi] \times [0, \pi] \times [0, \pi]$, the hyperbolic equation governing the wave propagation u is [19]

$$\frac{\partial^2 u}{\partial t^2} = \frac{\partial^2 u}{\partial x_1^2} + \frac{\partial^2 u}{\partial x_2^2} + \frac{\partial^2 u}{\partial x_3^2} - u, \quad ((x_1, x_2, x_3) \in \Omega, t \in [0, T]), \tag{86}$$

with the boundary conditions

$$u(0, x_2, x_3, t) = -u(\pi, x_2, x_3, t) = \sin x_2 \sin(x_3 + 2t), \tag{87}$$

$$u(x_1, 0, x_3, t) = -u(x_1, \pi, x_3, t) = \sin x_1 \sin(x_3 + 2t), \tag{88}$$

$$u(x_1, x_2, 0, t) = -u(x_1, x_2, \pi, t) = \sin(x_1 + x_2)\sin(2t), \tag{89}$$

and the initial conditions

$$u(x_1, x_2, x_3, 0) = \sin(x_1 + x_2)\sin(x_3), \tag{90}$$

$$\frac{\partial u(x_1, x_2, x_3, 0)}{\partial t} = 2\sin(x_1 + x_2)\cos(x_3). \tag{91}$$

The analytical solution used to compare with the approximate solution is

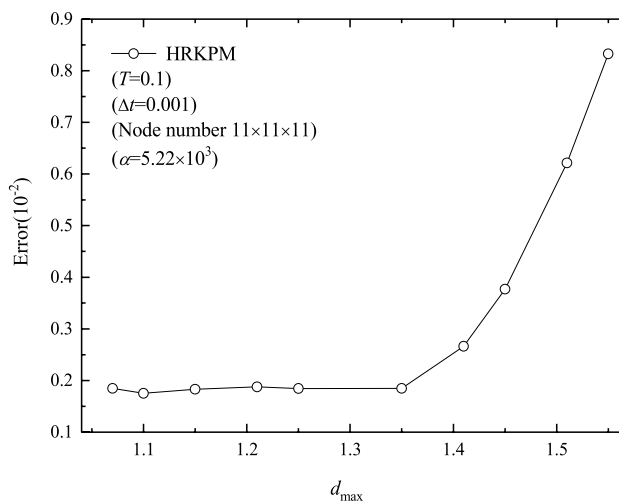$$u(x_1, x_2, x_3, t) = \sin(x_1 + x_2)\sin(x_3 + 2t). \tag{92}$$

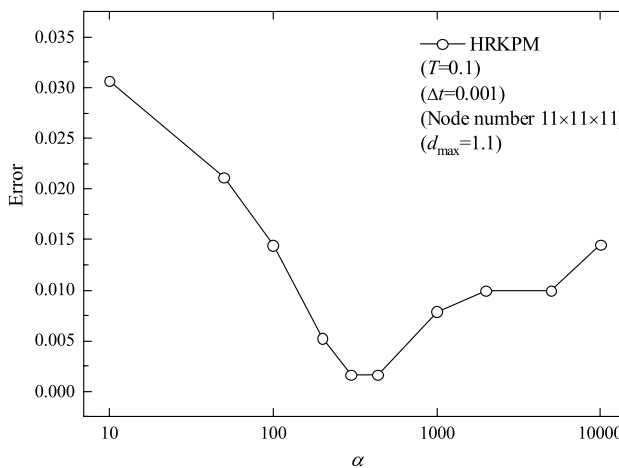**Fig. 2** Relative errors versus scale parameter $d_{\max}$

Fig. 3 Relative errors versus penalty factor α

In the HRKPM scheme for this example, we discuss factors that affect relative errors when x_3 is the selected splitting direction, such as the scale parameter of the influence domain $d_{\max}$, penalty factor α, the time step length Δt and node distribution. Figure 2 shows the relative errors of the HRKPM with different $d_{\max}$ when $\alpha = 5.22 \times 10^3$, $\Delta t = 0.001$, $T = 0.1$ and the node distribution is $11 \times 11 \times 11$. Figure 3 shows the relative errors of the HRKPM with different α when $d_{\max} = 1.1$, $\Delta t = 0.001$, $T = 0.1$ and the node distribution is $11 \times 11 \times 11$. Figure 4 shows the relative errors of the HRKPM with different Δt when $d_{\max} = 1.1$, $\alpha = 4.36 \times 10^2$, $T = 0.1$ and the node distribution is $11 \times 11 \times 11$. Figure 5 shows the relative errors of the HRKPM with different number of nodes when $d_{\max} = 1.1$, $\Delta t = 0.001$, $T = 0.1$, and l is the is the distance between adjacent nodes.
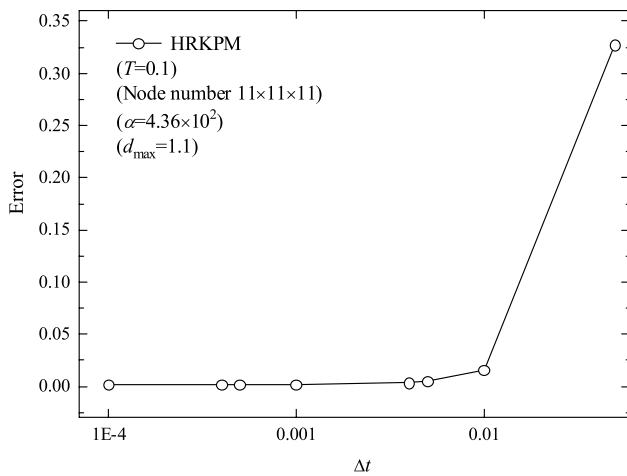
Fig. 4 Relative errors versus time step length Δt
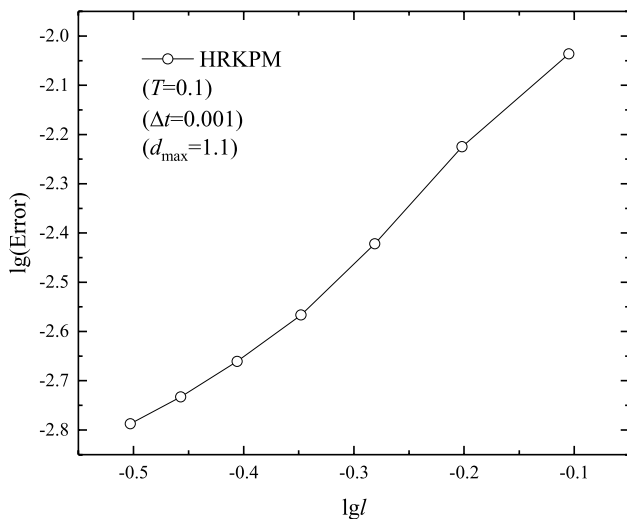

Fig. 5 Relative error versus the distance between adjacent nodes l

From Figs. 2 and 3, we can know that the HRKPM can obtain higher computational accuracy when d_{max} is in the interval from 1.07 to 1.5, α is in the interval from 2×10^2 to 1×10^3. It can be seen from Fig. 4 that when the time step length Δt is less than 0.001, the relative error tends to be stable. It can be seen from Fig. 5 that when there are more nodes in the domain, the distance between nodes is smaller, and the computational accuracy is higher. Therefore, the numerical result is convergent about the distance between nodes, and the order of convergence is 2.

In this example, we also use following polynomial basis [53]

$$\mathbf{p}^T(x_1, x_2) = (1, (x_1 - x_1')/h, (x_2 - x_2')/h), \tag{93}$$

where the fill distance h for a set of nodes $\{\mathbf{x}_i\}_{i=1}^M$ in the subdomain $\Omega^{(k)}$ can be defined as [10]

$$h = \sup_{\mathbf{x} \in \Omega^{(k)}} \min_{1 \le j \le M} \left\| \mathbf{x} - \mathbf{x}_j \right\|_2. \tag{94}$$

When the basis function in Eq. (93) is employed to the HRKPM, the factors affecting the relative errors, such as the scale parameter of the influence domain d_{max} and penalty factor α, are discussed. Figure 6 shows the relative errors of the HRKPM with different d_{max} when $\alpha = 4.4 \times 10^2$, $\Delta t = 0.001$, $T = 0.1$ and the node distribution is $11 \times 11 \times 11$. Figure 7 shows the relative errors of the HRKPM with different α when $d_{max} = 1.18$, $\Delta t = 0.001$, $T = 0.1$ and the node distribution is $11 \times 11 \times 11$. From Figs. 6 and 7, the HRKPM has higher computational accuracy when d_{max} is in the interval from 1.01 to 1.25, α is in the interval from 2×10^2 to 6×10^2.

Using the original basis function in Eq. (23) for this example, when $L = 10$, node distribution in each subdomain $\Omega^{(k)}$ is 11×11, $d_{max} = 1.1$, $\alpha = 4.36 \times 10^2$, $\Delta t = 0.001$ and $T = 0.1$, the relative error is 0.0016, the CPU time is 19.65. Using the basis function in Eq. (93) for this example, when $L = 10$, node distribution in each subdomain $\Omega^{(k)}$ is 11×11, $d_{max} = 1.18$, $\alpha = 4.74 \times 10^2$, $\Delta t = 0.001$ and $T = 0.1$, the relative error is 0.0082, the CPU time is 19.89. The comparison of the results shows that the original basis function can obtain higher computational accuracy than the basis function in Eq. (93). Therefore, the original basis function is used in this paper.

Table 1 lists the numerical results of the HRKPM, the RKPM and the EFG method at $T = 0.1$, $T = 0.3$ and $T = 0.5$. It is seen that the HRKPM can obtain more
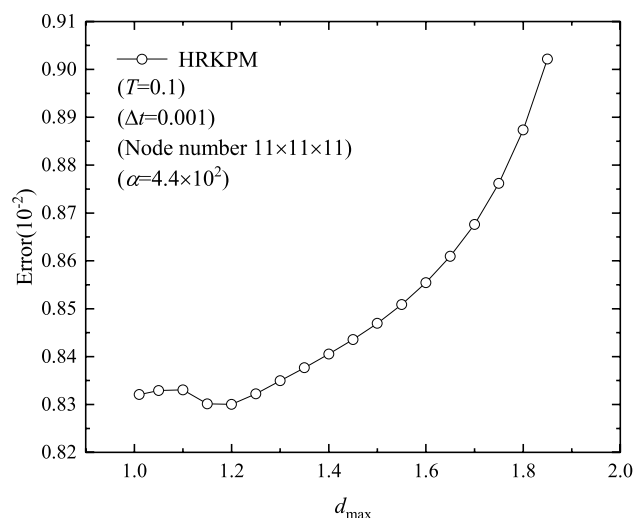

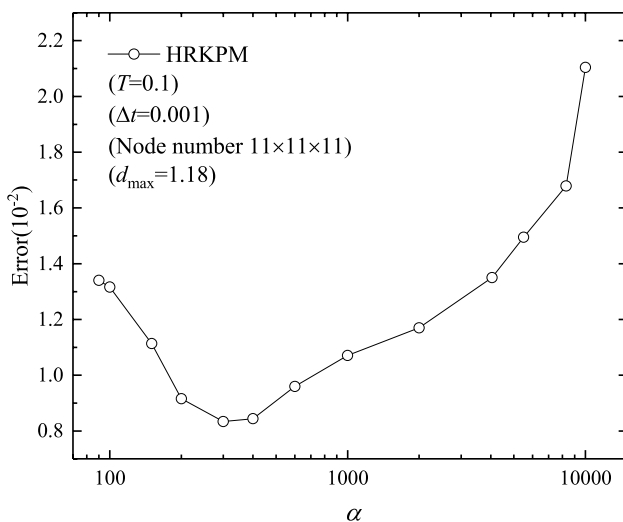**Fig. 6** Relative errors using the basis function in Eq. (93) versus scale parameter d_{max}

Fig. 7 Relative errors using the basis function in Eq. (93) versus penalty factor α

accurate and efficient numerical results. Especially when the time value is larger, the superiority of the HRKPM in computing speed is more obvious.

Table 2 shows the relative errors and CPU time of the HRKPM with different Gaussian points. From this table, we can see that when we choose more Gaussian points, the computational accuracy is improved, but the CPU time also increases. To balance the computational efficiency and the computational accuracy, we need to select the appropriate Gaussian points to compute the appeared integrals in Eqs. (55)–(60).

Figure 8 shows that the numerical solution obtained by the HRKPM, the RKPM and the EFG method are in good agreement with the analytical solution in the direction x_1, x_2 and x_3 at $T = 0.1$, $T = 0.3$ and $T = 0.5$. Compared with the RKPM and the EFG method, the HRKPM is implemented in a more time-saving way.

4.2 Wave propagation problem with mixed boundary conditions

In the 3D domain $\Omega = [0, \pi] \times [0, \pi] \times [0, \pi]$, the hyperbolic equation governing the wave propagation u is [19]

$$\frac{\partial^2 u}{\partial t^2} = 6\left(\frac{\partial^2 u}{\partial x_1^2} + \frac{\partial^2 u}{\partial x_2^2} + \frac{\partial^2 u}{\partial x_3^2}\right), \quad ((x_1, x_2, x_3) \in \Omega,\, t \in [0, T]), \tag{95}$$

with the boundary conditions

$$u(0, x_2, x_3, t) = u(\pi, x_2, x_3, t) = u(x_1, 0, x_3, t) = u(x_1, \pi, x_3, t) = 0, \tag{96}$$

$$\frac{\partial u(x_1, x_2, 0, t)}{\partial x_3} = \frac{\partial u(x_1, x_2, \pi, t)}{\partial x_3} = 0, \tag{97}$$

and the initial conditions

$$u(x_1, x_2, x_3, 0) = \sin x_1 \sin x_2 \cos(2x_3), \tag{98}$$

$$\frac{\partial u(x_1, x_2, x_3, 0)}{\partial t} = 0. \tag{99}$$

The analytical solution used to compare with the approximate solution is

$$u(x_1, x_2, x_3, t) = \sin x_1 \sin x_2 \cos(2x_3) \cos(6t). \tag{100}$$

In the HRKPM scheme for this example, the discussion about different types of boundary conditions is applied.

1. When Neumann boundary condition exists in the splitting direction
   Set x_3 as splitting direction, the boundary conditions in this direction are $\frac{\partial u(x_1, x_2, 0)}{\partial x_3} = 0$ and $\frac{\partial u(x_1, x_2, \pi)}{\partial x_3} = 0$. It means that the smaller Δx_3 is, the closer the value of u on plane $x_3 = 0$ is to that on plane $x_3 = \Delta x_3$, and the closer the value of u on plane $x_3 = \pi$ is to that on plane $x_3 = \pi - \Delta x_3$.
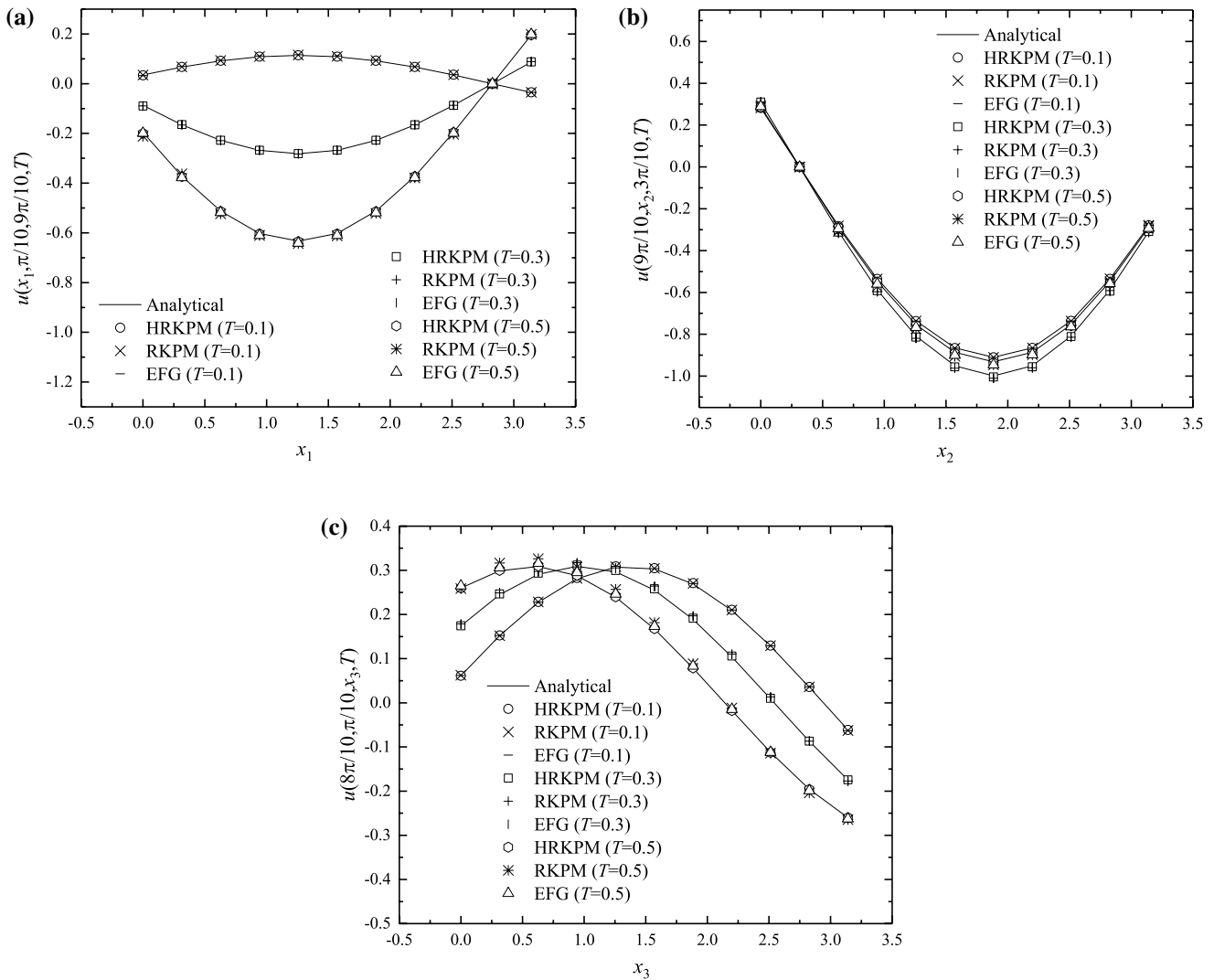
Table 1 The relative errors and CPU time of the HRKPM, the RKPM and the EFG method at different times

Time	Relative error			CPU time		
	HRKPM	RKPM	EFG	HRKPM	RKPM	EFG
$T = 0.1$	0.0016	0.0031	0.0035	19.65	425.88	245.67
$T = 0.3$	0.0046	0.011	0.0090	50.7	1182.17	678.87
$T = 0.5$	0.0095	0.0156	0.012	84.11	2013.66	1338.3

Table 2 The relative errors and CPU time of the HRKPM with different Gaussian points

Gaussian points	4×4	5×5	6×6	7×7	8×8	9×9
Relative error	0.001632	0.001601	0.001596	0.001588	0.001592	0.001595
CPU time	19.65	27.713	38.227	48.347	50.632	59.634

Fig. 8 Wave propagation obtained by the HRKPM, the RKPM and the EFG method **a** in the direction x_1; **b** in the direction x_2 and **c** in the direction x_3

When $L = 100$, node distribution in each subdomain is 11×11, $d_{max} = 1.05$, $\alpha = 1.01 \times 10^4$, $\Delta t = 0.001$ and $T = 0.1$, the relative error is 0.0062, the computing time is 15.82.

2. When Dirichlet boundary condition exists in the splitting direction

Set x_2 as splitting direction, the boundary conditions in this direction are $u(x_1, 0, x_3, t) = 0$ and $u(x_1, \pi, x_3, t) = 0$, which are exactly the values of u on plane $x_2 = 0$ and $x_2 = \pi$, respectively.

When $L = 10$, node distribution in each sudomain is 11×11, $d_{max} = 1.23$, $\alpha = 1.7 \times 10^3$, $\Delta t = 0.001$ and $T = 0.1$, the relative error is 0.0024, the computing time is 1.1.

According to the above description and discussion, better results are obtained when Dirichlet boundary condition is set as the splitting direction. Therefore, to obtain higher accuracy, it is necessary to choose more suitable splitting direction according to boundary conditions.

We employ the HRKPM, the RKPM and the EFG method to solve this 3D example. A good agreement between the numerical solutions obtained by these methods and the analytical solution are shown in Fig. 9 when $T = 0.1$ and $T = 0.5$. Moreover, the HRKPM has higher numerical efficiency, which is exactly what we want to achieve with the proposed method.
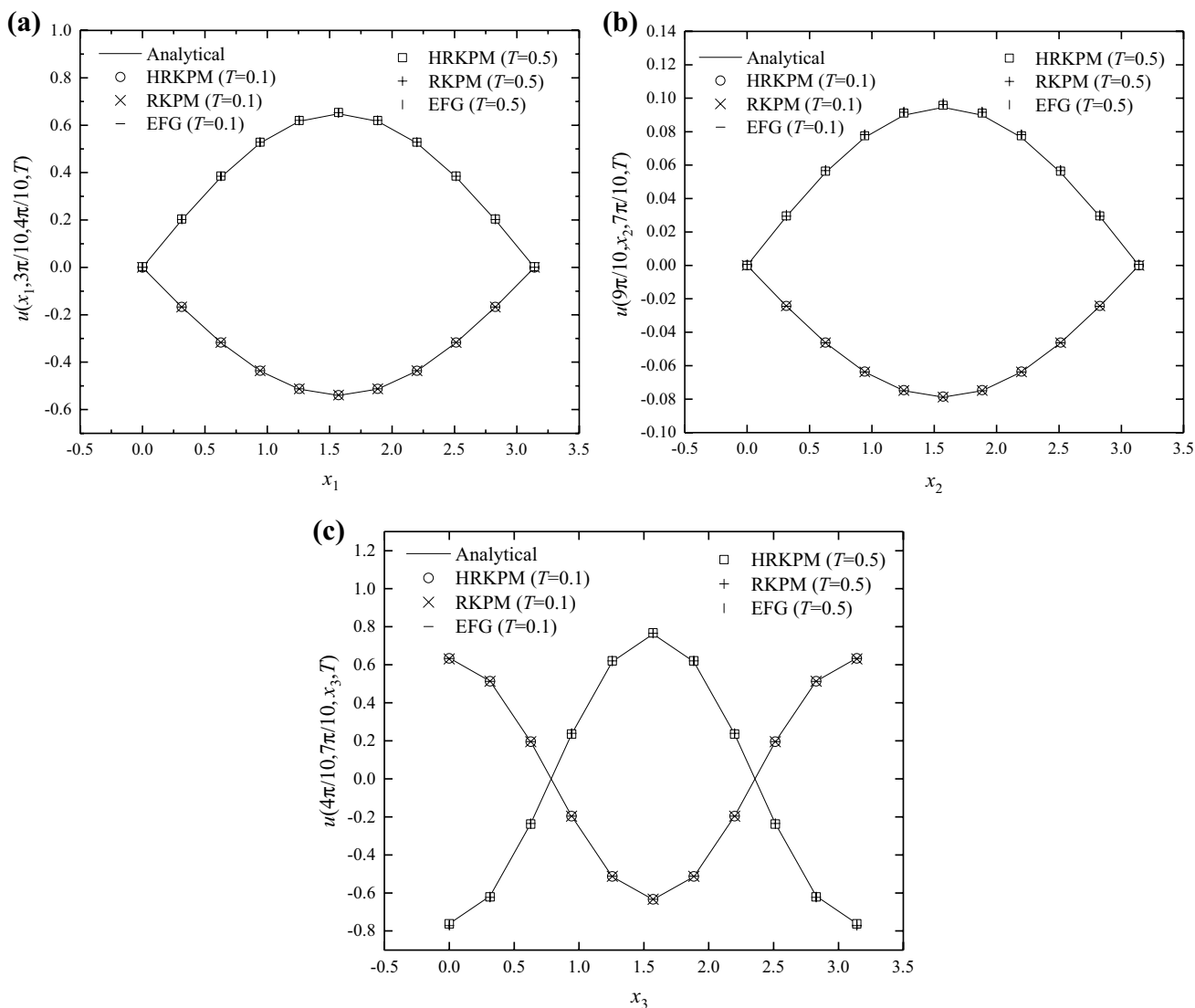
Fig. 9 Wave propagation obtained by the HRKPM, the RKPM and the EFG method **a** in the direction x_1; **b** in the direction x_2 and **c** in the direction x_3

4.3 Wave propagation problem in cylindrical coordinates

Consider the following equation in cylindrical coordinates [50]

$$\frac{\partial^2 u}{\partial t^2} = \frac{\partial^2 u}{\partial r^2} + \frac{\partial^2 u}{\partial \theta^2} + \frac{\partial^2 u}{\partial x_3^2} + u, \quad (r \in [1,2], \ \theta \in [0,\pi], \ x_3 \in [0,1]), \tag{101}$$

with the boundary conditions

$$u(1, \theta, x_3, t) = (\sin\theta + x_3) \cdot e^t, \tag{102}$$

$$T(2, \theta, x_3, t) = x_3 \cdot e^t, \tag{103}$$

$$T(r, 0, x_3, t) = x_3 \cdot e^t, \tag{104}$$

$$T(r, \pi, x_3, t) = x_3 \cdot e^t, \tag{105}$$

$$T(r, \theta, 0, t) = \frac{4}{3}\left(\frac{1}{r} - \frac{r}{4}\right)\sin\theta \cdot e^t, \tag{106}$$

$$T(r, \theta, 1, t) = \left[\frac{4}{3}\left(\frac{1}{r} - \frac{r}{4}\right)\sin\theta + 1\right] \cdot e^t, \tag{107}$$

and the initial conditions

$$u(r, \theta, x_3, 0) = \frac{\partial u(r, \theta, x_3, 0)}{\partial t} = \frac{4}{3}\left(\frac{1}{r} - \frac{r}{4}\right)\sin\theta + x_3. \tag{108}$$

The analytical solution used to compare with the approximate solution is

$$u(r, \theta, x_3, t) = \left[\frac{4}{3} \left(\frac{1}{r} - \frac{r}{4} \right) \sin \theta + x_3 \right] \cdot e^t. \tag{109}$$

In the HRKPM scheme for this example, the step number in the selected splitting direction x_3 is 20, the node distribution in each 2D subdomain $\Omega^{(k)}$ is 9×31. The arrangement of nodes can be shown in Fig. 10. Using the RKPM and the EFG method for this example, the node distribution in the 3D domain Ω is $9 \times 31 \times 21$.

Table 3 lists the numerical results obtained by the HRKPM, the RKPM and the EFG method at $T = 0.01$, $T = 0.03$ and $T = 0.05$. We can observe that the HRKPM has higher computational accuracy and efficiency. Especially when the time value is larger, the superiority of the HRKPM in computing speed is more obvious.

We employ the HRKPM, the RKPM and the EFG method to solve this 3D example. A good agreement between the numerical solutions obtained by these methods and the analytical solution are shown in Fig. 11. Again, the HRKPM has higher computational efficiency than the RKPM and the EFG method for solving 3D wave propagation problems.

For randomly node distribution in each subdomain, as shown in Fig. 12, when the node distribution is $9 \times 31 \times 21$, the relative errors of the HRKPM, the RKPM and the EFG method are 4.6×10^{-4}, 0.0011 and 0.001, respectively. The CPU times are 28.5, 780.53 and 515.67, respectively. Based on the results, we can know that the HRKPM can also obtain higher computational efficiency than the RKPM and the EFG method with randomly node distribution.
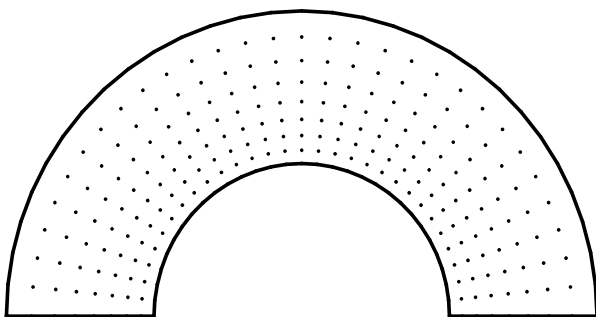

Fig. 10 Node distribution in 2D subdomain of a half torus

The numerical solutions in the directions r, θ and x_3 obtained by the HRKPM, the RKPM and the EFG method with randomly node distribution are presented in Fig. 13. And these numerical solutions are in agreement with the analytical one.

4.4 Wave propagation problem with non-smooth solution

In the 3D domain $\Omega = [0, \pi] \times [0, \pi] \times [0, \pi]$, the hyperbolic equation governing the wave propagation u is

$$\frac{\partial^2 u}{\partial t^2} = \frac{\partial^2 u}{\partial x_1^2} + \frac{\partial^2 u}{\partial x_2^2} + \frac{\partial^2 u}{\partial x_3^2} + \cos x_1 + \cos x_2,$$
$$((x_1, x_2, x_3) \in \Omega, t \in [0, T]), \tag{110}$$

with the boundary conditions

$$\frac{\partial u(0, x_2, x_3, t)}{\partial x_1} = \frac{\partial u(\pi, x_2, x_3, t)}{\partial x_1} = \frac{\partial u(x_1, 0, x_3, t)}{\partial x_2}$$
$$= \frac{\partial u(x_1, \pi, x_3, t)}{\partial x_2} = 0, \tag{111}$$

$$u(x_1, x_2, 0, t) = u(x_1, x_2, \pi, t) = \cos x_1 + \cos x_2, \tag{112}$$

and the initial conditions

$$u(x_1, x_2, x_3, 0) = \cos x_1 + \cos x_2, \tag{113}$$

$$\frac{\partial u(x_1, x_2, x_3, 0)}{\partial t} = \begin{cases} \sin x_3 & x_1 < \frac{8}{10}\pi \\ 5 \sin 5x_3 & x_1 \geq \frac{8}{10}\pi \end{cases}. \tag{114}$$

The analytical solution used to compare with the approximate solution is

$$u(x_1, x_2, x_3, t) = \begin{cases} \cos x_1 + \cos x_2 + \sin x_3 \cdot \sin t & x_1 < \frac{8}{10}\pi \\ \cos x_1 + \cos x_2 + \sin 5x_3 \cdot \sin 5t & x_1 \geq \frac{8}{10}\pi \end{cases}. \tag{115}$$

Using the HRKPM scheme for this example, when $L = 10$, the node distribution in each subdomain $\Omega^{(k)}$ is 11×11, $d_{max} = 1.5$, $\Delta t = 0.01$ and $T = 0.1$, the relative error is 0.0036, the CPU time is 11.12. Using the RKPM scheme for this example, when the node distribution in 3D domain Ω is $11 \times 11 \times 11$, $d_{max} = 1.21$, $\alpha = 2.7 \times 10^2$, $\Delta t = 0.01$ and
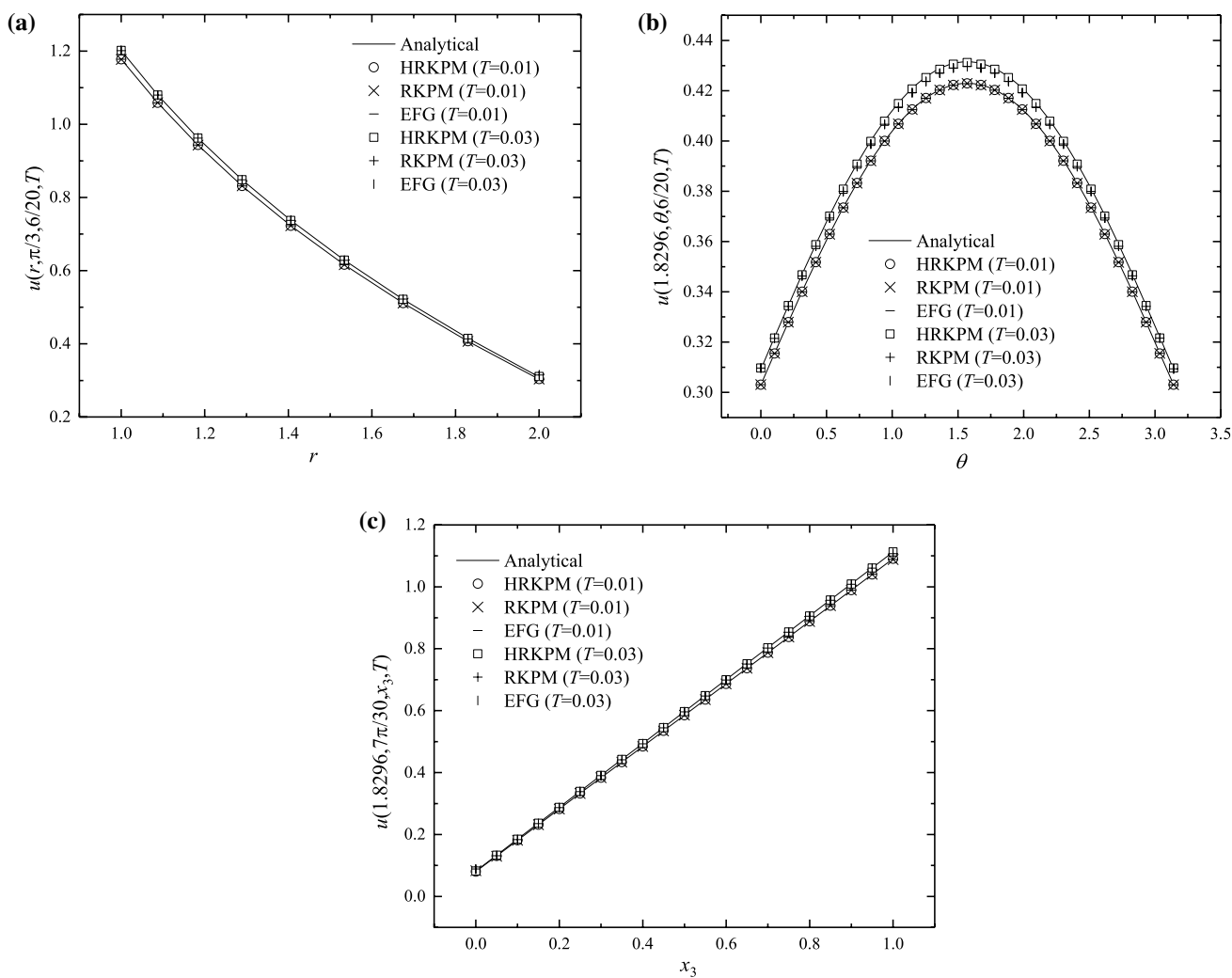
Table 3 The relative errors and CPU time of the HRKPM, the RKPM and the EFG method at different times

Time	Relative error			CPU time		
	HRKPM	RKPM	EFG	HRKPM	RKPM	EFG
$T = 0.01$	4.54×10^{-4}	0.0011	0.0010	21.3	685.18	472.93
$T = 0.03$	6.77×10^{-4}	0.0042	0.0038	55.74	1031.72	714.29
$T = 0.05$	7.25×10^{-4}	0.01	0.0103	91.51	1479.43	1019.12

Fig. 11 Wave propagation obtained by the HRKPM, the RKPM and the EFG method **a** in the direction r; **b** in the direction θ and **c** in the direction x_3
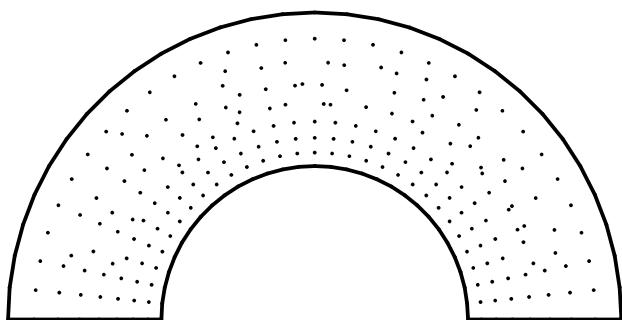

Fig. 12 Randomly distribution in 2D subdomain of a half torus

$T = 0.1$, the relative error is 0.0037, the CPU time 118.1. Using the EFG method for this example, when the node distribution in 3D domain Ω is $11 \times 11 \times 11$, $d_{\max} = 1.01$, $\alpha = 2.6 \times 10^2$, $\Delta t = 0.01$ and $T = 0.1$, the relative error is 0.0052, the CPU time is 36.04. From these results, it can be seen that the HRKPM is more efficient than the RKPM and the EFG method.

We employ the HRKPM, the RKPM and the EFG method to solve this 3D example. A good agreement between the numerical solutions obtained by these methods and the analytical solution are shown in Fig. 14. Again, the HRKPM has higher computational efficiency than the RKPM and the EFG method for solving 3D wave propagation problems.
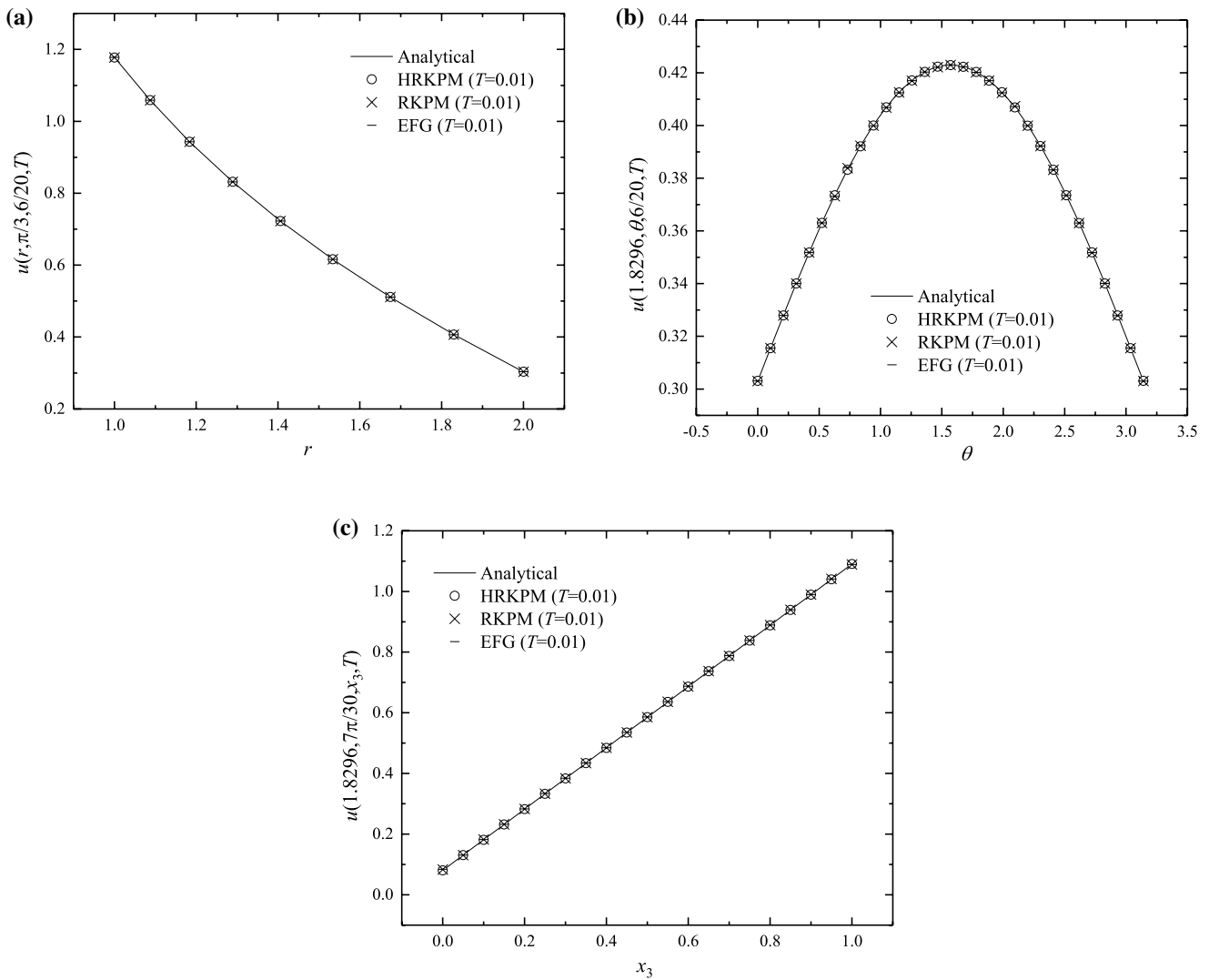
(a)

(b)

(c)

Fig. 13 Wave propagation obtained by the HRKPM, the RKPM and the EFG method **a** in the direction r; **b** in the direction θ and **c** in the direction x_3

5 Conclusions

This paper studies the HRKPM for solving 3D wave propagation problems. Four selected numerical examples are used to evaluate the effectiveness and superiority of the proposed method. Compared with the RKPM and the EFG method, the following conclusions can be obtained:

1. The HRKPM has greater computational precision when $d_{\max}$ is in the interval from 1.07 to 1.5, α is in the interval from 2×10^2 to 1×10^3, the number of nodes increase or the time step length decrease. Moreover, the proper splitting direction is also one of the factors affecting the calculation accuracy.

2. The HRKPM greatly improves the computational efficiency. Especially when the time value is larger, the superiority of HRKPM in computing speed is more obvious.
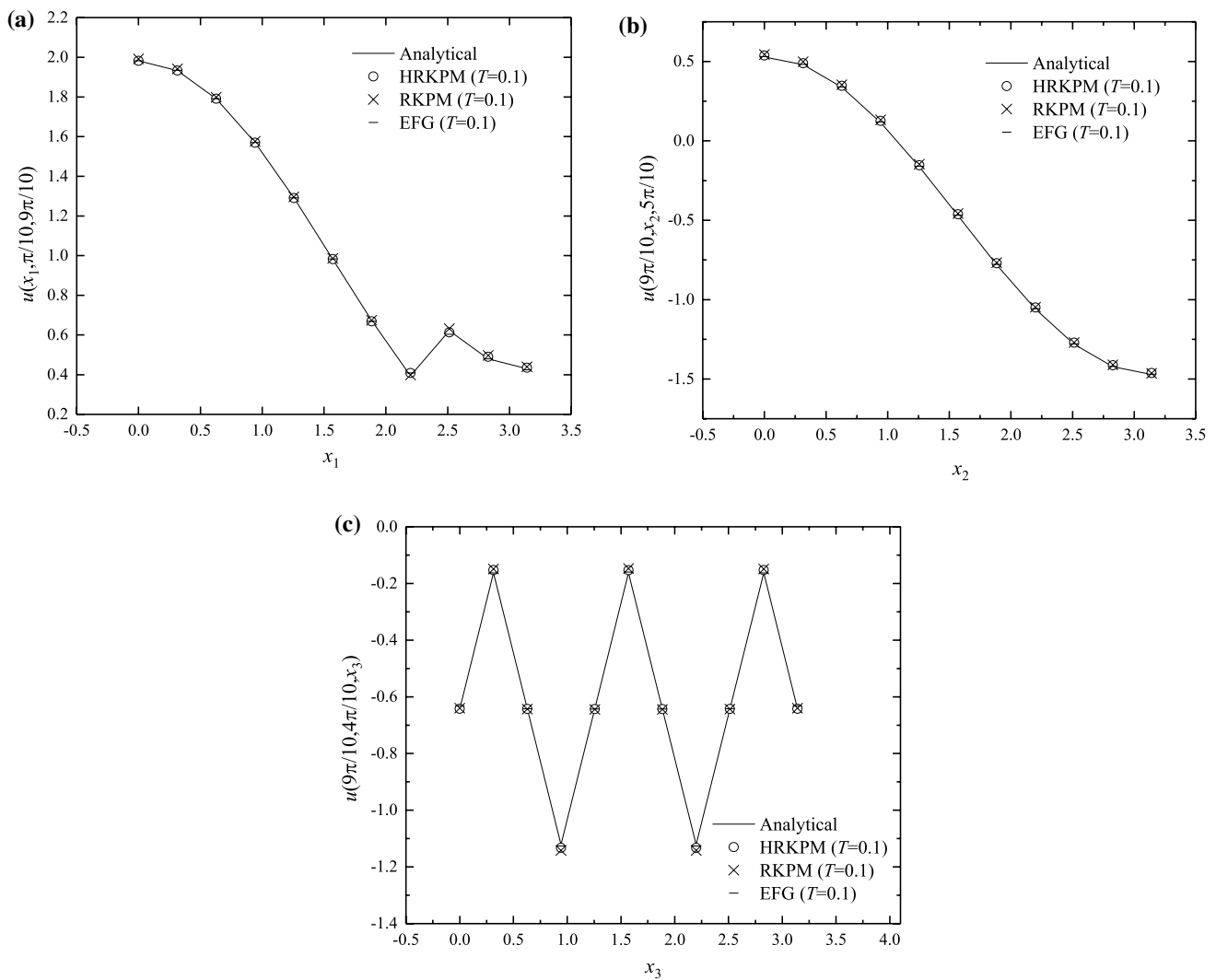
Fig. 14 Wave propagation obtained by the HRKPM, the RKPM and the EFG **a** in the direction x_1; **b** in the direction x_2 and **c** in the direction x_3

References

1. Kadalbajoo MK, Kumar A, Tripathi LP (2015) A radial basis functions based finite differences method for wave equation with an integral condition. Appl Math Comput 253:8–16
2. Wang S, Virta K, Kreiss G (2016) High order finite difference methods for the wave equation with non-conforming grid interfaces. J Sci Comput 68(3):1002–1028
3. Dehghan M (2005) On the solution of an initial-boundary value problem that combines Neumann and integral condition for the wave equation. Numer Methods Partial Differ Equ 21:24–40
4. Dehghan M (2006) Finite difference procedures for solving a problem arising in modeling and design of certain optoelectronic devices. Math Comput Simul 71:16–30
5. Ainsworth M, Monk P, Muniz W (2006) Dispersive and dissipative properties of discontinuous Galerkin finite element methods for the second-order wave equation. J Sci Comput 27(1–3):5–40
6. Chen X, Birk C, Song C (2015) Transient analysis of wave propagation in layered soil by using the scaled boundary finite element method. Comput Geotech 63:1–12
7. Huang R, Zheng SJ, Liu ZS, Ng TY (2020) Recent advances of the constitutive models of smart materials-hydrogels and shape memory polymers. Int J Appl Mech 12(2):2050014
8. Cheng YM (2015) Meshless methods. Science Press, Beijing
9. Cheng YM, Wang WQ, Peng MJ, Zhang Z (2014) Mathematical aspects of meshless methods. Math Probl Eng 2014:756297

10. Salehi R, Dehghan M (2013) A generalized moving least square reproducing kernel method. J Comput Appl Math 249:120–132

11. Abbaszadeh M, Dehghan M (2019) The reproducing kernel particle Petrov–Galerkin method for solving two-dimensional nonstationary incompressible Boussinesq equations. Eng Anal Bound Elem 106:300–308

12. Liu FB, Cheng YM (2018) The improved element-free Galerkin method based on the nonsingular weight functions for elastic large deformation problems. Int J Comput Mater Sci Eng 7(3):1850023

13. Liu FB, Wu Q, Cheng YM (2019) A meshless method based on the nonsingular weight functions for elastoplastic large deformation problems. Int J Appl Mech 11(1):1950006

14. Dehghan M, Narimani N (2018) An element-free Galerkin meshless method for simulating the behavior of cancer cell invasion of surrounding tissue. Appl Math Model 59:500–513

15. Dehghan M, Narimani N (2020) The element-free Galerkin method based on moving least squares and moving Kriging approximations for solving two-dimensional tumor-induced angiogenesis model. Eng Comput 36(4):1517–1537

16. Qin XQ, Duan XB, Hu G, Su LJ, Wang X (2018) An Element-free Galerkin method for solving the two-dimensional hyperbolic problem. Appl Math Comput 321:106–120

17. Cheng RJ, Ge HX (2012) Meshless method for a kind of three-dimensional hyperbolic equation. Appl Mech Mater 101–102:1126–1129

18. Cheng RJ, Ge HX (2009) Element-free Galerkin (EFG) method for a kind of two-dimensional linear hyperbolic equation. Chin Phys B 18:4059–4064

19. Zhang Z, Li DM, Cheng YM, Liew KM (2012) The improved element-free Galerkin method for three-dimensional wave equation. Acta Mech Sin 28(3):808–818

20. Shivanian E (2015) Meshless local Petrov–Galerkin (MLPG) method for three-dimensional nonlinear wave equations via moving least squares approximation. Eng Anal Bound Elem 50:249–257

21. Shivanian E, Shaban M (2019) An improved pseudospectral meshless radial point interpolation (PSMRPI) method for 3D wave equation with variable coefficients. Eng Comput 35(4):1159–1171

22. Liew KM, Cheng RJ (2013) Numerical study of the three-dimensional wave equation using the mesh-free kp-Ritz method. Eng Anal Bound Elem 37:977–989

23. Dehghan M, Salehi R (2012) A method based on meshless approach for the numerical solution of the two-space dimensional hyperbolic telegraph equation. Math Methods Appl Sci 35:1120–1233

24. Dehghan M, Salehi R (2012) A meshless based numerical technique for traveling solitary wave solution of Boussinesq equation. Appl Math Model 36:1939–1956

25. Liu WK, Jun S, Zhang YF (1995) Reproducing kernel particle methods. Int J Numer Methods Eng 20:1081–1106

26. Cheng RJ, Ge HX (2010) Meshless analysis of three-dimensional steady-state heat conduction problems. Chin Phys B 19(9):090201

27. Cheng RJ, Liew KM (2012) A meshless analysis of three-dimensional transient heat conduction problems. Eng Anal Bound Elem 36:203–210

28. Ma JC, Gao HF, Wei GF, Qiao JW (2020) The meshless analysis of wave propagation based on the Hermit-type RRKPM. Soil Dyn Earthq Eng 134:106154

29. Dehghan M, Abbaszadeh M (2017) A local meshless method for solving multi-dimensional Vlasov–Poisson and Vlasov–Poisson–Fokker–Planck systems arising in plasma physics. Eng Comput 33(4):961–981

30. Dehghan M, Abbaszadeh M (2017) Element free Galerkin approach based on the reproducing kernel particle method for solving 2D fractional Tricomi-type equation with Robin boundary condition. Comput Math Appl 73(6):1270–1285

31. Cheng J (2020) Analyzing the factors influencing the choice of the government on leasing different types of land uses: evidence from Shanghai of China. Land Use Policy 90:104303

32. Cheng J (2020) Data analysis of the factors influencing the industrial land leasing in Shanghai based on mathematical models. Math Probl Eng 2020:9346863

33. Chen L, Cheng YM (2010) The complex variable reproducing kernel particle method for elasto-plasticity problems. Sci China Phys Mech Astron 53(5):954–965

34. Chen L, Ma HP, Cheng YM (2013) Combining the complex variable reproducing kernel particle method and the finite element method for solving transient heat conduction problems. Chin Phys B 22(5):050202

35. Chen L, Cheng YM, Ma HP (2015) The complex variable reproducing kernel particle method for the analysis of Kirchhoff plates. Comput Mech 55(3):591–602

36. Chen L, Cheng YM (2018) The complex variable reproducing kernel particle method for bending problems of thin plates on elastic foundations. Comput Mech 62:67–80

37. Weng YJ, Zhang Z, Cheng YM (2014) The complex variable reproducing kernel particle method for two-dimensional inverse heat conduction problems. Eng Anal Bound Elem 44:36–44

38. Weng YJ, Cheng YM (2013) Analysis of variable coefficient advection–diffusion problems via complex variable reproducing kernel particle method. Chin Phys B 22(9):090204

39. Li KT, Huang AX, Zhang WL (2002) A dimension split method for the 3D compressible Navier Stokes equations in turbomachine. Commun Numer Methods Eng 18:1–14

40. Li KT, Liu DM (2009) Dimension splitting method for 3D rotating compressible Navier–Stokes equations in the turbomachinery. Int J Numer Anal Model 6:420–439

41. Li KT, Shen XQ (2007) A dimensional splitting method for the linearly elastic shell. Int J Comput Math 84(6):807–824

42. Bragin MD, Rogov BV (2016) On exact dimensional splitting for a multidimensional scalar quasilinear hyperbolic conservation law. Dokl Math 94:382–386

43. Cheng H, Peng MJ, Cheng YM (2017) A fast complex variable element-free Galerkin method for three-dimensional wave propagation problems. Int J Appl Math 9(6):1750090

44. Cheng H, Peng MJ, Cheng YM (2017) A hybrid improved complex variable element-free Galerkin method for three-dimensional potential problems. Eng Anal Bound Elem 84:52–62

45. Cheng H, Peng MJ, Cheng YM (2018) The dimension splitting and improved complex variable element-free Galerkin method for 3-dimensional transient heat conduction problems. Int J Numer Methods Eng 114:321–345

46. Cheng H, Peng MJ, Cheng YM (2018) A hybrid improved complex variable element-free Galerkin method for three-dimensional advection–diffusion problems. Eng Anal Bound Elem 97:39–54

47. Cheng H, Peng MJ, Cheng YM (2020) A hybrid complex variable element-free Galerkin method for 3D elasticity problems. Eng Struct 219:110835

48. Meng ZJ, Cheng H, Ma LD, Cheng YM (2018) The dimension split element-free Galerkin method for three-dimensional potential problems. Acta Mech Sin 34(3):462–474

49. Meng ZJ, Cheng H, Ma LD, Cheng YM (2019) The dimension splitting elementfree Galerkin method for 3D transient heat conduction problems. Sci China Phys Mech Astron 62(4):040711

50. Meng ZJ, Cheng H, Ma LD, Cheng YM (2019) The hybrid element-free Galerkin method for three-dimensional wave propagation problems. Int J Numer Methods Eng 117:15–37

51. Peng PP, Wu Q, Cheng YM (2020) The dimension splitting reproducing kernel particle method for three-dimensional potential problems. Int J Numer Methods Eng 121:146–164

52. Fang DY (2008) Nonlinear wave equation. Zhejiang University Press, Zhejiang
53. Li XL, Li SL (2016) On the stability of the moving least squares approximation and the element-free Galerkin method. Comput Math Appl 72:1515–1531